BRAIN CONNECTIVITY
Volume XX, Number XX, 2018

DOI: 10.1089/brain.2017.0547

ORIGINAL ARTICLE

Enhanced Brain Network Activity in Complex Movement Rhythms: A Simultaneous Functional Magnetic Resonance Imaging and Electroencephalography Study

Bhim M. Adhikari,[1,2] Charles M. Epstein,[3] and Mukesh Dhamala[1,4–7]

Abstract

Generating movement rhythms is known to involve a network of distributed brain regions associated with motor planning, control, execution, and perception of timing for the repertoire of motor actions. What brain areas are bound in the network and how the network activity is modulated by rhythmic complexity have not been completely explored. To contribute to answering these questions, we designed a study in which nine healthy participants performed simple to complex rhythmic finger movement tasks while undergoing simultaneous functional magnetic resonance imaging and electroencephalography (fMRI-EEG) recordings of their brain activity during the tasks and rest. From fMRI blood oxygenation-level-dependent (BOLD) measurements, we found that the complexity of rhythms was associated with brain activations in the primary motor cortex (PMC), supplementary motor area (SMA), and cerebellum (Cb), and with network interactions from these cortical regions to the cerebellum. The spectral analysis of single-trial EEG source waveforms at the cortical regions further showed that there were bidirectional interactions between PMC and SMA, and the complexity of rhythms was associated with power spectra and Granger causality spectra in the beta (13–30 Hz) frequency band, not in the alpha (8–12 Hz) and gamma (30–58 Hz) bands. These results provide us new insights into the mechanisms for movement rhythm complexity.

Keywords: directed connectivity; Granger causality; information flow; rhythmic finger tapping; sensorimotor

Introduction

Rhythm refers to the division of time through distinct order and patterns of events, objects, symbols, or signs. Rhythm formation can integrate basic levels of sensory perception and motor entrainment into complex cognitive processes and motor adaptations (Thaut et al., 1999a). We can recognize, discriminate, generate, and maintain a large number of rhythms and synchronize motor movements with an external rhythmic cue (Haken, 1996; Kelso, 1995). Timing or frequency of movements determines the stability of synchronization. Complexity of multifrequency motor rhythms is generally characterized by the ratios of frequencies or time intervals involved. Several important aspects of the neurobiology of the rhythms such as neural representation of integer and noninteger ratio rhythms (Sakai et al., 1999), neural correlates of the motor rhythm complexity (Dhamala et al., 2003), brain activity with temporal complexity of rhythms (Lewis et al., 2004), neural correlates of rhythmic versus discrete movements (Schaal et al., 2004), and the neural basis of human dance (Brown et al., 2006) were revealed. Furthermore, neuroimaging studies have lately begun to investigate the neurobiological basis of motor rhythm generation (Brown et al., 2006; Dhamala et al., 2003; Lewis et al., 2004; Sakai et al., 1999; Schaal et al., 2004; Verstynen et al., 2005). Several studies have demonstrated that rhythmic synchronization is an effective tool for rehabilitation in patients with Parkinson's disease (Arias and Cudeiro, 2008; Howe et al., 2003; McIntosh et al., 1997; Prassas et al., 1997; Rochester et al., 2009; Thaut et al., 1996), traumatic brain injury (Hurt et al., 1998; Kenyon and Thaut, 2000), spinal cord injury (de l'Etoile, 2008), stroke (Hayden et al., 2009;

[1]Department of Physics and Astronomy, Georgia State University, Atlanta, Georgia.
[2]Department of Psychiatry, Maryland Psychiatric Research Center, University of Maryland School of Medicine, Baltimore, Maryland.
[3]Department of Neurology, Emory University School of Medicine, Atlanta, Georgia.
[4]Neuroscience Institute, Georgia State University, Atlanta, Georgia.
Centers for [5]Behavioral Neuroscience, [6]Nano-Optics, and [7]Diagnostics and Therapeutics, Georgia State University, Atlanta, Georgia.

Roerdink et al., 2007, 2009), Huntington's disease (Thaut et al., 1999b), and in patients with cerebellar ataxia (Abiru et al., 2008).

Recent advances in neuroimaging techniques have enabled us to acquire simultaneous recordings with multiple modalities. Noninvasive neuroimaging techniques can be divided into two groups based on their measurement principles: electrophysiological measurement, such as electroencephalography (EEG) and magnetoencephalography (MEG), and hemodynamic measurement, such as functional magnetic resonance imaging (fMRI) and near-infrared spectroscopy (NIRS). EEG/MEG record millisecond changes in brain electrical but have poor spatial resolution, while fMRI/NIRS can provide spatial localization of activity within millimeters but are suffered from the slow vascular response limiting their temporal resolution (Fazli et al., 2012).

The multimodal approach can overcome these limits by complementing each signal (Biessmann et al., 2011; Friston, 2009; Shibasaki, 2008). Simultaneous fMRI-EEG data recording solve the problem to get high spatial and temporal resolution to study the brain dynamics in an efficient manner and give us information about the brain activity and networks (de Souza et al., 2013; Meyer et al., 2011; Novitskiy et al., 2011; Ostwald et al., 2011). Even in well-established cognitive experiments, the behavior of the same participant in the same task can differ substantially between EEG and fMRI recording sessions (Ullsperger and von Cramon, 2001), as EEG recordings are carried out in a sound-attenuated chamber and upright position, whereas fMRI blood oxygenation-level-dependent (BOLD) signals are recorded in a bit noisy MRI environment and a supine position. The advantage of simultaneous fMRI-EEG recordings lies clearly in otherwise inevitable differences of subject preparation, data acquisition, and variable behavioral outcomes between separate recording sessions (Ullsperger, 2010). Simultaneous protocols not only guarantee identical sensory stimulation, perception, behavior, and avoid order or repetition effects (Debener et al., 2006) but also provide a unique way to study how these intrinsic brain states interact with event-related, extrinsic processing. More recent developments in amplifier design, and artifact-correction procedures now make it much easier to obtain reasonable EEG data quality (Debener et al., 2007; Iannetti et al., 2005; Niazy et al., 2005; Sammer et al., 2005).

The brain signals from fMRI and/or EEG measurements can be used to extract large-scale brain connectivity patterns. The information of functional interaction obtained by a symmetric measure such as cross-correlation has been referred to as functional connectivity (Friston et al., 1993). Granger causality (GC) (Granger, 1969, 1980) can be used to estimate directed functional connectivity. This technique is based on the notion of linear prediction of one signal by incorporating the past information of another signal. This approach does not require any assumption of prior connectivity structures as required in structural equation modeling (Buchel and Friston, 1997; McIntosh and Gonzalez-Lima, 1994), nonlinear system identification techniques (Friston and Buchel, 2000), and Bayesian estimation of deterministic state-space models (Friston et al., 2003). GC methods have been successfully applied to electrophysiological animal data (Baccala and Sameshima, 2001; Bernasconi and König, 1999; Bernasconi et al., 2000; Brovelli et al., 2004; Liang et al., 2000, 2017), human EEG data (Hesse et al., 2003; Kaminski et al., 2001), and human fMRI data (Goebel et al., 2003, 2004; Harrison et al., 2003; Sato et al., 2006). Recently, a model-free, copula-based GC method has been applied to both simulations and neural data (Hu and Liang, 2014).

Here we designed a rhythmic finger-tapping (RFT) task with different beat complexities and collected high-quality simultaneous fMRI-EEG signals. The present study aimed at applying GC to BOLD signals to investigate the pattern of directed interactions within the regions involved in the generation of motor rhythms and examine the interaction patterns using the EEG source signals from the cortical brain activation regions of the sensorimotor network. We also compared the oscillatory activity of these nodes at rest and RFT task. We applied GC methods to extract complementary information from fMRI-EEG simultaneous recordings about the brain activity flow patterns among motor regions during RFT task.

Materials and Methods

Participants

There were nine participants (eight males, one female; mean age ± standard deviation = 26.6 ± 4.1 years), who completed all the three simultaneous fMRI-EEG recording sessions. All participants had normal or corrected to normal vision and reported normal neurological history. Participants provided signed informed consent forms and were compensated for their participation in the experiment. The Institutional Review Board of Georgia State University approved the study.

Data acquisition and analysis

Before setting up for simultaneous fMRI-EEG acquisition, participants were informed about the details of the task and took part in a practice session to familiarize them with the task. Following the EEG setup, participants were briefly explained on the basic principles of EEG and how to minimize introducing contaminants into the ongoing EEG signals. The experiment consisted of three functional runs, each run had the durations for rest and RFT tasks. Each run was 8-min long, during which the subject was asked to rest (equivalently, 0 beat rhythm) for a minute and perform RFT on a response box with different beat rhythms (1, 2, and 3), a minute each. The visual cues were 0 for motor-resting condition or for 0-beat rhythm (B_0), 1 for 1-beat rhythm (B_1), 2 for 2-beat rhythm (B_2), and 3 for 3-beat rhythm (B_3). During the presentation of 0, subjects were asked to keep their right index finger in contact with the button maintaining a slight pressure but without any movement. Each visual cue (0, 1, 2, or 3) appeared twice, a minute each in randomized sequence within a run. The task trial sequence was displayed and randomized using stimulus software presentation (www.neurobs.com).

EEG was recorded using an MRI-compatible EEG system with a 68-channel electrode cap, AgCl sintered electrodes, and SynAmps2 amplifiers at a sampling rate of 10 kHz/channel (Neuroscan Systems, Charlotte, NC). Analog-to-digital conversion was performed at a resolution of 24 bits. The electrode cap was aligned to standard cranial fiducials and exploring electrodes were referenced against the right mastoid. Electrode impedances were kept below 10 kΩ. An fMRI pulse was used as a trigger to simultaneously start

the stimulus presentation for displaying visual cues and EEG recordings.

The EEG data, contaminated by gradient artifacts due to magnetic field gradients, and ballistocardiogram (BCG) artifacts due to cardiac pulsations, were processed in BrainVision Analyzer 2 (Brain Products, Germany), which detected and corrected the EEG artifacts. During the preprocessing step, the average of the recorded EEG data was used as a new reference (average reference). MR-induced artifacts in the EEG signal were subtracted from the raw data using standard inbuilt algorithms (Allen et al., 1998, 2000). The MR-gradient artifact (obtained by utilizing the repetitiveness of the artifact shape to form an average artifact template) was removed and the data were downsampled to 200 Hz, with a low-pass filter, 58 Hz, with 48 as the slope for finite impulse response filter before pulse artifact correction. The cardioballistic artifact caused by movement due to heartbeat was subtracted from the EEG data. QRS complexes of the heartbeat were semiautomatically identified in the BCG channel, which showed a clearly detectable R-peak. Since the cardioballistic artifact is highly variable across time, subtraction templates were continuously recalculated using a sliding average. After the corrections for gradient and cardioballistic artifacts, the data were low-pass filtered at 58 Hz to attenuate high-frequency noise and then an independent component analysis was performed to eliminate artifacts of eye movements, eye blinks, muscle activity, and residual MR artifacts.

Besides these corrections, data from each recording session from each individual subject were thoroughly inspected visually and data from bad electrodes were discarded and replaced, when appropriate, by spatial interpolation of the recordings from the neighboring working electrodes. The preprocessed data were then imported using MATLAB-interface in Analyzer and read in EEGLAB format, and later separated into data segments for B_0, B_1, B_2, and B_3 based on behavioral trial sequences. These trial segments were used to reconstruct the EEG source waveforms using the minimum norm estimate (MNE) technique, one of the inverse solution approaches (Hamalainen and Ilmoniemi, 1994; Wang et al., 1992). The MNE estimates the source activity without *a priori* assumption about the sources' location and activity. In this study, we selected the cortical brain activation loci derived from fMRI images.

fMRI data

The whole-brain MRI was done on a 3-Tesla Siemens scanner in the Biomedical Imaging Technology Center at Emory University, Atlanta, GA. The functional scans were acquired with T_2*-weighted gradient echo-planar imaging protocol with the following parameters: echo time (TE) = 32 ms, repetition time (TR) = 2000 ms, flip angle = 90°, voxel size = $3 \times 3 \times 4\,mm^3$, field of view = 256×256 mm, matrix size = 64×64, and 33 axial slices each of 5 mm thickness. High-resolution anatomical images were acquired using a magnetization-prepared rapid gradient-echo sequence with the parameters: TR = 2300 ms, TE = 2.91 ms, flip angle = 9°, and voxel size = $1 \times 1 \times 1\,mm^3$. Statistical Parametric Mapping 8 (SPM8) (www.fil.ion.ucl.ac.uk/spm) software was used for preprocessing the fMRI data. We performed the following steps: slice timing correction, motion correction, coregistration to individual anatomical image, and then normalization to Montreal Neurological Institute (MNI) template (Friston et al., 1995). The voxels were resized to $3 \times 3 \times 3\,mm^3$ per voxel resolution. Spatial smoothing of the normalized image was done with an 8-mm full-width at half-maximum isotropic Gaussian kernel.

A random-effect, model-based, univariate statistical analysis was performed in a two-level procedure. At the first level, a separate general linear model (GLM) was specified as per the task sequences. In GLM analysis, the conditions: B_0, B_1, B_2, B_3, and six motion parameters were included. The six motion parameters, entered as nuisance covariates, were regressed out of the data. Individual contrast images from the first-level analysis were then entered and a second-level analysis for a separate one-sample *t*-test. The summary statistical maps thus obtained were then thresholded [($p < 0.001$, uncorrected; a cluster size ($k > 10$)] and overlaid on high-resolution structural image in MNI orientation. We then performed multiple comparison correction on all activation t-maps using Monte Carlo simulation implemented in AFNI (Cox, 1996) (AFNI 3dClusterSim http://afni.nih.gov/afni/doc/manual/3dclust.pdf) (Cox et al., 2016).

Connectivity analysis-fMRI

The regions of interest (ROIs) were based on brain activation t-maps from task versus rest contrast. We defined three ROIs, by generating a sphere of 6 mm radius. The center coordinates were (−45, −16, 52) for the left primary motor cortex (LPMC), (0, −1, 61) for the supplementary motor area (SMA), and (21, −49, −26) for the right cerebellum (RCb). The time courses from all the voxels within each ROI and all subjects were extracted for each experimental task and rest blocks. We performed GC analysis to characterize the directional influences between these ROIs.

For each ROI data, we constructed hidden neural signals by hemodynamic deconvolution as done in previous studies (David et al., 2008; Handwerker et al., 2004; Roebroeck et al., 2011; Valdes-Sosa et al., 2011; Wu et al., 2013). The reason behind this is fMRI-BOLD signals are believed to be originated from smoothing of neuronal activity by the hemodynamic response function (Aguirre et al., 1998; Handwerker et al., 2004). The segmented deconvolved BOLD time series after removing the ensemble-mean separately from each voxel and subject were treated as trials for reliable estimates of the network measures. We calculated the GC spectra by the parametric approach (Dhamala et al., 2008). To find significance level of GC, we constructed surrogate data sets by randomly permuting trial or segment order from each participant and task condition, computed GC from each data set, built a distribution of maximum GC values, and estimated the threshold for significant GC as in previous studies (Blair and Karniski, 1993; Brovelli et al., 2004). The threshold was thus based on the null hypothesis that there was no statistical interdependence between nodes when trials were randomized. We computed GC spectra from all possible pairs of ROIs with a minimum of 1000 random permutations per task condition and picked maximum GC on each permutation. The threshold value for GC spectra at significance $p < 10^{-6}$ was obtained by fitting the distribution with a gamma-distribution function and this threshold value was used to identify significantly active directed network activity among ROIs calculated in pairwise GC

analysis. We applied conditional GC analysis to differentiate direct and indirect connections between three nodes to address the drawbacks of GC analyses as stated in previous fMRI and EEG connectivity studies (Hesse et al., 2003; Roelstraete and Rosseel, 2012). We ruled out the mediated interactions and retained only the direct network interactions. We also computed the time-domain GC values for significantly active network directions from each participant and performed paired *t*-tests to find the significant network modulation during the task conditions in comparison to rest.

Connectivity analysis-EEG

We computed task-related activations from fMRI data. We used the information of the brain activations into the source modeling analysis of EEG data. As the activation foci derived from fMRI images can be used to guide the placement of dipole locations (Liu et al., 2006), we selected the cortical activation loci primary motor cortex (PMC) and SMA as reliable EEG sources. We did not consider Cb activation as a source in the EEG source modeling since Cb is a deeper brain source. We fitted the dipoles at fMRI peak activation locations [Talairach coordinates: (−45, −16, 48) for PMC and (0, 2, 56) for SMA with dipole orientations (0.2, −1.0, 0.2) and (0.1, 1.0, 0.1), respectively]. Using the minimum norm estimate approach, one of the inverse solution techniques, in Brain Electrical Source Analysis Research software version 6.0 (www.besa.de), we obtained EEG source waveforms. For this, we used single-trial EEG data from different rhythm task blocks and obtained corresponding single-trial source waveforms from the fitted dipoles at the abovementioned locations and the dipole orientations. The source signals thus obtained were used to calculate spectral measures for the network activity analysis.

We calculated wavelet-based spectral power and parametric spectral measures: coherence and GC. The same procedures,

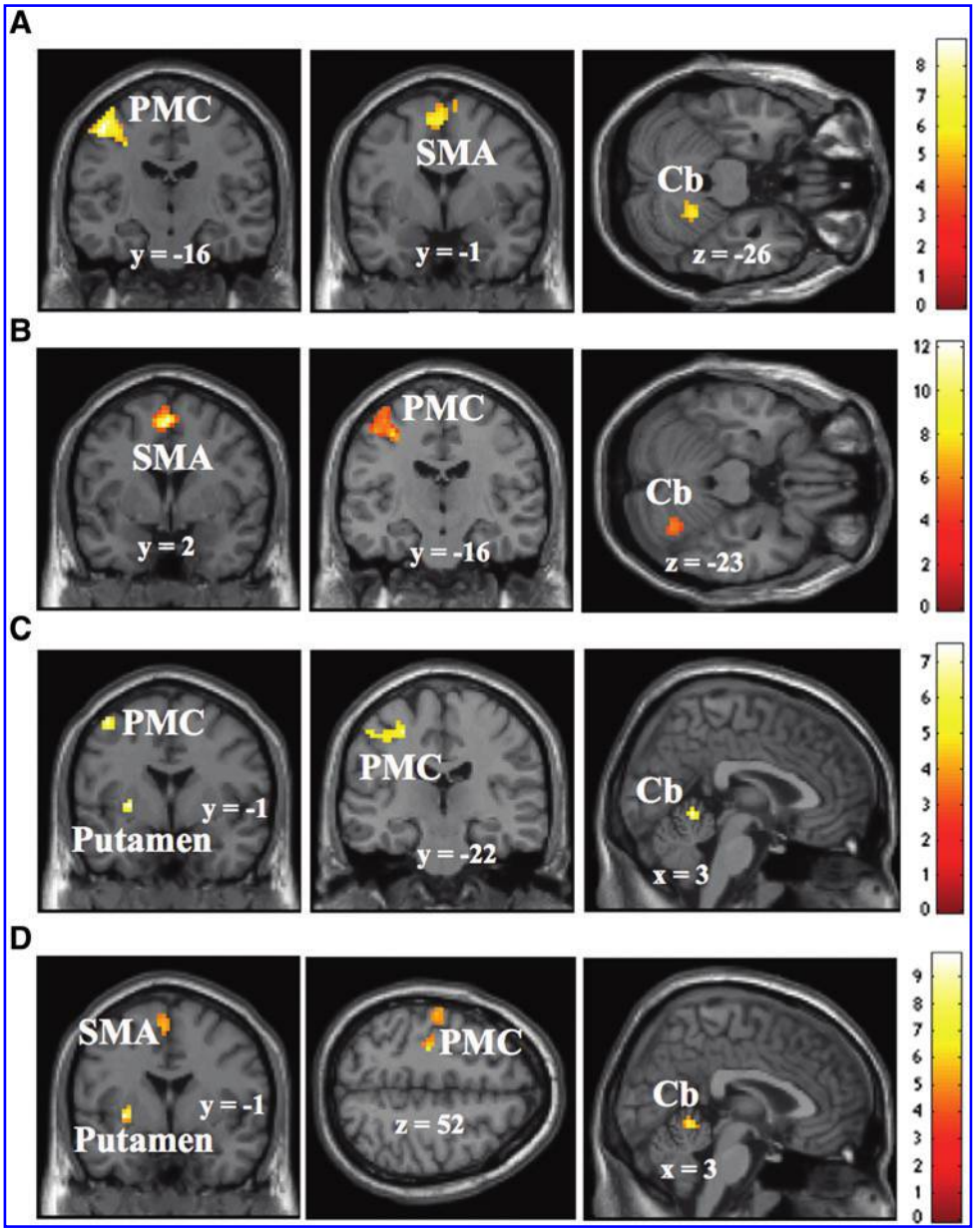

FIG. 1. Brain activations: The brain activations shown are for RFT tasks versus rest (0-beat rhythm) **(A)**, for 1-beat rhythm versus rest **(B)**, for 2-beat rhythm versus rest **(C)**, and for 3-beat rhythm versus rest **(D)**. The color intensity represents t-statistics, and the activations are overlaid on the MNI structural template brain in neurological orientation. Cb, cerebellum; PMC, primary motor cortex (pre/postcentral gyrus); RFT, rhythmic finger tapping; SMA, supplementary motor area. Color images available online at www.liebertpub.com/brain

Table 1. Brain Activations for Various Contrasts

Contrast	*Brain region*	*Cluster size*	*Voxel* t *(z-equivalent)*	*MNI coordinates* x, y, z
Task>rest	L PMC***	196	8.84 (4.25)	−45, −16, 52
			6.89 (3.84)	−30, −19, 43
			6.70 (3.79)	−33, −25, 58
	SMA**	47	6.62 (3.77)	0, −1, 61
			5.77 (3.53)	9, 2, 64
	R Cb*	32	6.23 (3.66)	21, −49, −26
B_1>B_0	SMA***	79	12.19 (4.76)	0, 2, 58
			5.14 (3.32)	9, 5, 64
	L PMC***	195	7.84 (4.05)	−33, −16, 49
			6.84 (3.82)	−33, −10, 55
			6.23 (3.66)	−48, −10, 52
	R Cb$^{n.s.}$	12	5.76 (3.52)	30, −64, −23
B_2>B_0	L Putamen*	11	7.49 (3.98)	−27, −1, 1
	R Cb*	11	6.85 (3.82)	3, −52, −5
	L PMC*	11	6.78 (3.81)	−42, −1, 58
	L PMC***	56	6.52 (3.74)	−27, −22, 52
			6.28 (3.67)	−51, −16, 52
			5.84 (3.55)	−39, −25, 46
B_3>B_0	L Putamen**	18	9.83 (4.42)	−27, −1, −2
	R Cb*	15	7.66 (4.01)	3, −52, −5
	L PMC***	66	7.11 (3.89)	−27, −22, 52
			5.57 (3.47)	−42, −13, 64
			5.54 (3.46)	−51, −16, 52
	L SMA*	17	6.16 (3.64)	−3, −1, 61

It includes information about anatomical locations, cluster sizes, *t*-value (z-score), and MNI coordinates for the activations under statistical significance $p<0.001$ and cluster extent $k>10$. The t-map of each contrast is corrected for multiple comparisons using Monte Carlo simulation implemented in AFNI (Cox, 1996) (AFNI 3dClusterSim http://afni.nih.gov/afni/doc/manual/3dclust.pdf). The individual voxel probability threshold is set to be 0.05.

*$p<0.05$; **$p<0.01$; ***$p<0.001$.

B_0, 0-beat rhythm (rest); B_1, 1-beat rhythm; B_2, 2-beat rhythm; B_3, 3-beat rhythm; Cb, cerebellum; L, left; MNI, Montreal Neurological Institute; n.s., not significant; PMC, primary motor cortex (pre/postcentral gyrus); R, right; SMA, supplementary motor area.

as performed in fMRI time series, were followed for the EEG source waveforms to determine the model order that better described the data and used for spectral calculation. The thresholds for statistical significance $p<10^{-3}$ were computed from surrogate data using permutation tests and a gamma-function fit.

Results

Brain activations

Figure 1 shows the fMRI activation maps for the duration when participants performed the RFT tasks: B_1, B_2, and B_3, and during rest (B_0). The tapping task versus rest contrast showed activations in LPMC, SMA, and RCb (Fig. 1A). B_1 versus B_0 contrast showed the activation in SMA, LPMC, and RCb (Fig. 1B), whereas B_2 versus B_0 showed activations in left putamen in addition to RCb and the LPMC (Fig. 1C). Similarly, B_3 versus B_0 showed activation in the left putamen, RCb, LPMC, and SMA (Fig. 1D). These activations were initially subjected to a cluster-forming threshold $p<0.001$ and cluster size, $k>10$. We performed multiple comparison correction on all activation t-maps using Monte Carlo simulation implemented in AFNI (Cox, 1996) (AFNI 3dClusterSim http://afni.nih.gov/afni/doc/manual/3dclust.pdf) (Cox et al., 2016). The activations that survived significance of corrected $p<0.05$ are marked with asterisk "*", "**" for corrected $p<0.01$, "***" for corrected $p<0.001$ as shown in Table 1.

BOLD response

Analysis was carried out to examine how node activity changes during finger tapping versus rest contrast, B_1-B_0, B_2-B_0, and B_3-B_0. We calculated the average region-specific beta (β) values for LPMC, RCb, and SMA during these conditions in the tapping tasks. The node activities, as indicated by β-values, were significantly higher ($p<0.05$) for B_3-B_0 compared with B_2-B_0 and B_1-B_0 for all nodes as shown in Figure 2. There were no significant differences in node activities when β-values for B_2-B_0 were compared with β-values for B_1-B_0. The details of the statistical test results are given in Table 2a.

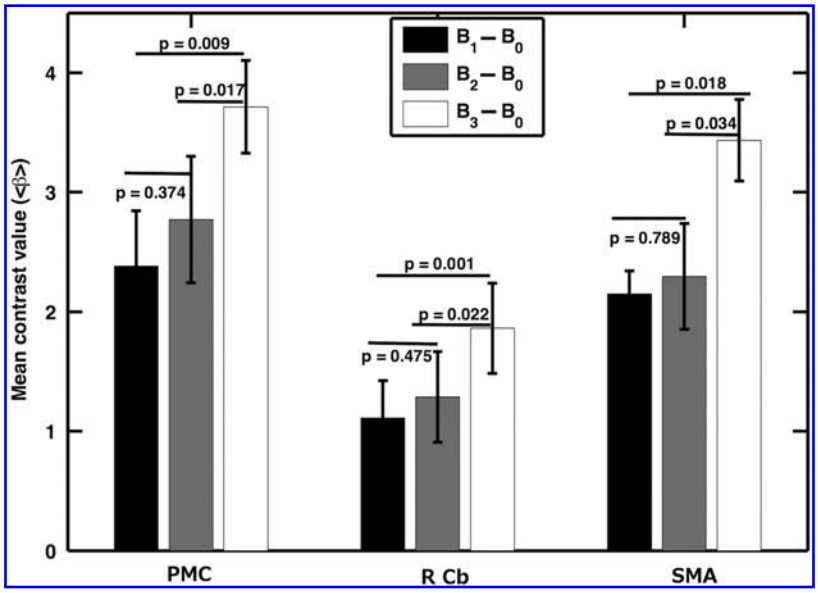

FIG. 2. Comparison between contrast values: contrast values (<β>) were calculated for (B_1-B_0), (B_2-B_0), and (B_3-B_0) from LPMC, RCb, and SMA. Here B_0: 0-beat rhythm, B_1: 1-beat rhythm, B_2: 2-beat rhythm, and B_3: 3-beat rhythm. The error bar represents the standard error of the mean. LPMC, left primary motor cortex; RCb, right cerebellum; SMA, supplementary motor area.

Table 2. The Statistical Significance Level for Beta Contrast Value Comparison and Power Comparison for Beat Rhythms

(a) Contrast values and their statistical test scores for different beat rhythms

	<β>			p-*value*/t-*value*		
Regions	$B_1 > B_0$	$B_2 > B_0$	$B_3 > B_0$	$(B_2 > B_0)$ *vs.* $(B_1 > B_0)$	$(B_3 > B_0)$ *vs.* $(B_2 > B_0)$	$(B_3 > B_0)$ *vs.* $(B_1 > B_0)$
PMC	2.38	2.77	3.71	0.374/0.94	***0.017/3.02***	***0.009/3.42***
R Cb	1.12	1.29	1.86	0.475/0.74	***0.022/2.84***	***0.001/5.02***
SMA	2.16	2.31	3.44	0.79/0.28	***0.034/2.56***	***0.018/2.97***

(b) Statistical test scores for power comparison for different beat rhythms

	PMC			*SMA*		
Regions	B_1 *vs.* B_0	B_2 *vs.* B_0	B_3 *vs.* B_0	B_1 *vs.* B_0	B_2 *vs.* B_0	B_3 *vs.* B_0
Alpha-band *p*-value/*t*-value	0.64/0.48	0.39/–0.90	0.24/–1.27	0.74/–0.35	0.43/–0.83	0.18/–1.47
Beta-band *p*-value/*t*-value	0.34/–1.09	***0.034/–2.56***	***0.021/−2.87***	0.94/0.09	***0.041/–2.44***	***0.033/−2.58***

Bold values represent that statistical significance level, $p < 0.05$.

Network activity

We computed the pairwise-GC spectra to assess network interactions among the three nodes: LPMC, RCb, and SMA (nodes were selected based on task versus rest contrast) for button presses that included the time series for B_1, B_2, and B_3. The permutation threshold criteria were followed to find the significant causal interaction directions (for details, see the Materials and Methods section). The significant causal connections among these nodes (represented schematically) are shown in Figure 3A. The interaction directions between two nodes are direct and are not mediated by the remaining third node. The numerical values are the peak GC values from the GC spectra and represent the strength of the causal interactions. During RFT tasks, we found the bidirectional causal interactions between PMC and SMA, unidirectional causal influences from PMC and SMA to Cb.

From the GC-spectra for B_0, B_1, B_2, and B_3 of each participant, we calculated the time-domain GC values, integrating the entire frequency range (0.0185–0.25 Hz). When we compared the causal influences between B_1 and B_0, we found that there was a significant increase ($p < 0.05$) in

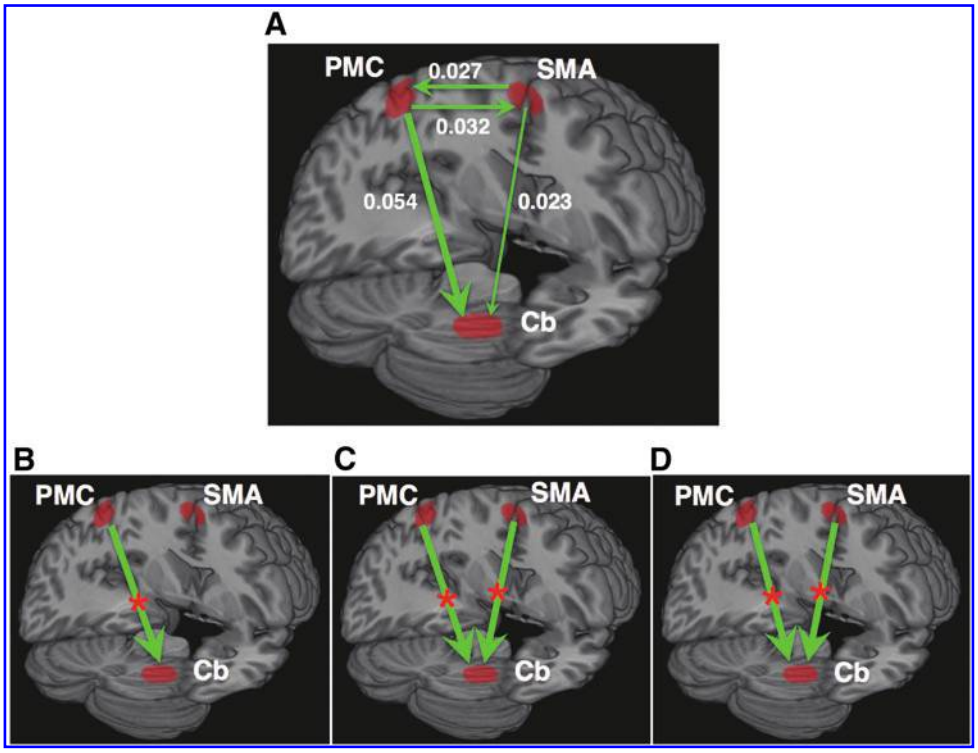

FIG. 3. Network interactions: Schematic representation of significant causal interaction directions among three nodes: LPMC, SMA, and RCb. The significant causal connections for RFT tasks (all beats), as determined by using permutation threshold criteria ($p < 10^{-6}$), are shown in **(A)** by green line with an arrowhead; the width of the line represents the connection strength (maximum GC value), thicker the line, stronger the causal influence. The red stars represent the significant increase in network interaction directions ($p < 0.05$) when the causal strengths during **(B)** 1-beat rhythm, **(C)** 2-beat rhythm, and **(D)** 3-beat rhythm are compared with the causal strengths during rest. GC, Granger causality. Color images available online at www.liebertpub.com/brain

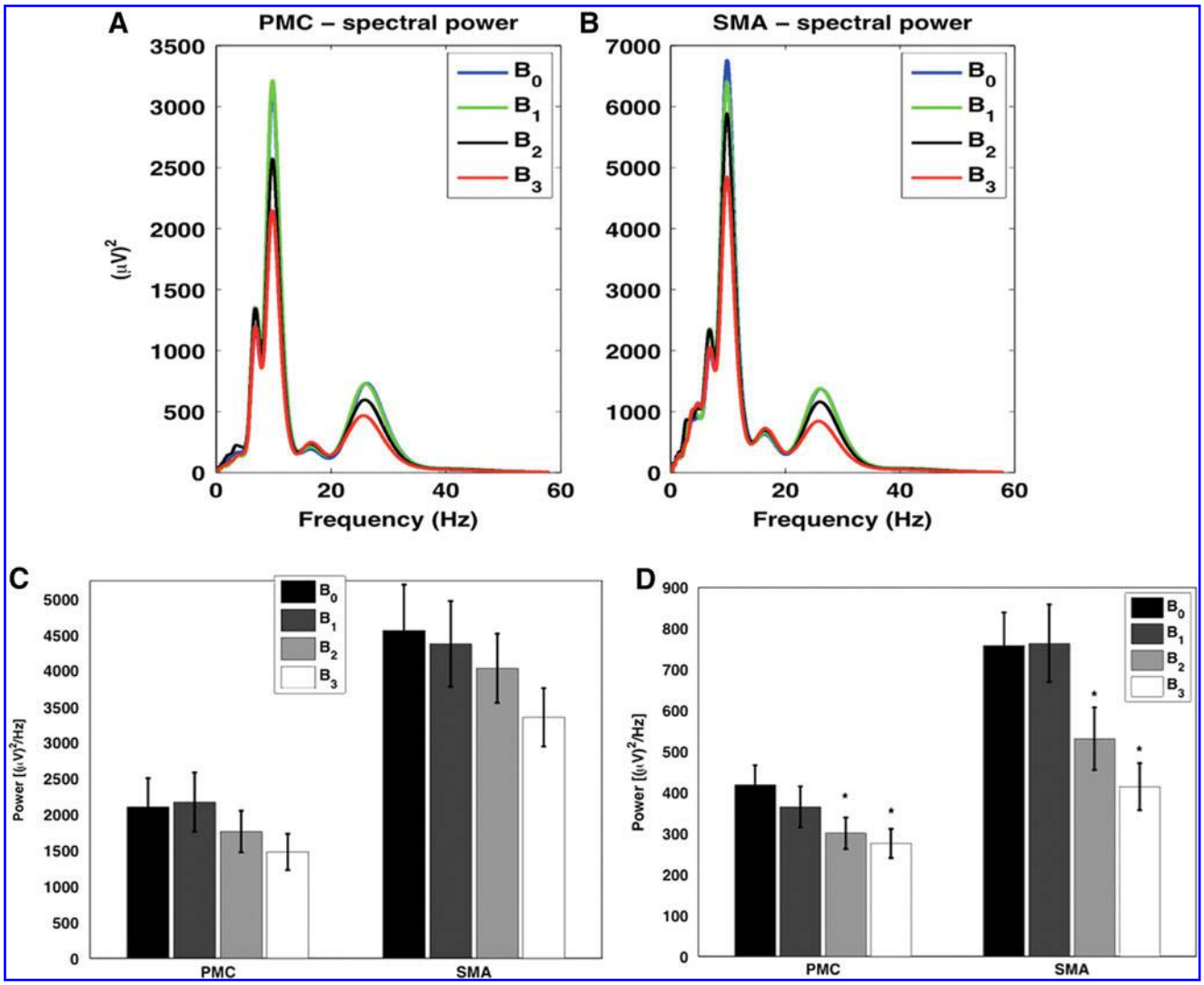

FIG. 4. EEG spectral power and power differences: Upper panel shows spectral power for rest (0-beat rhythm, B_0), and finger tapping tasks (B_1: 1-beat rhythm, B_2: 2-beat rhythm, and B_3: 3-beat rhythm) from PMC **(A)** and SMA **(B)** respectively. Lower panel shows the average α-band (8–12 Hz) power **(C)** and β-band (13–30 Hz) power **(D)** for PMC and SMA for different beat rhythms. The significant difference ($p < 0.05$) in power is marked with asterisk (*) during button presses in comparison with rest. EEG, electroencephalography. Color images available online at www.liebertpub.com/brain

causal influence from PMC to Cb (Fig. 3B). The causal influences increased significantly ($p < 0.05$) from PMC to Cb and from SMA to Cb during B_2 and B_3 compared with B_0 (Fig. 3C, D). Here a significant increase in causal influence is marked with a star (*).

EEG artifact preprocessing

This study consisted of a total of 27 runs, 3 data recording sessions per subject. Each recording session consisted of two 1-min segments for each rhythm (B_0, B_1, B_2, and B_3) and hence it is of an 8-min length. During artifact preprocessing, we excluded the two data segments from two subjects, a segment each for B_0 and B_3 for a subject and a segment for each B_1 and B_2 for the next subject. The number of interpolated electrodes varied from 1 to 12 in these 27 recording sessions, with the mean (±standard deviation) 7 (±2).

fMRI-constrained EEG analysis

The single-trial source waveforms for fMRI-constrained cortical sources, PMC and SMA, were used to compute the spectral power. Considering all source waveforms from all participants, we found spectral peaks at ~10 Hz (α-range), ~16 Hz, and ~26 Hz (β-range), the peak at ~26 Hz had a higher magnitude for both nodes (Fig. 4A, B) in all conditions. No changes in α-band (8–12 Hz) node activities were found for both nodes during task conditions compared to rest (Fig. 4C). However, we found a significant decrease ($p < 0.05$) in β-band (13–30 Hz) node activities during B_2 and B_3 compared with B_0 (Fig. 4D). The statistical details are given in Table 2b.

From the pairwise-GC spectral calculation using single-trial source waveforms for button presses and the permutation threshold criteria as described in the Materials and Methods section, we found bidirectional causal interactions,

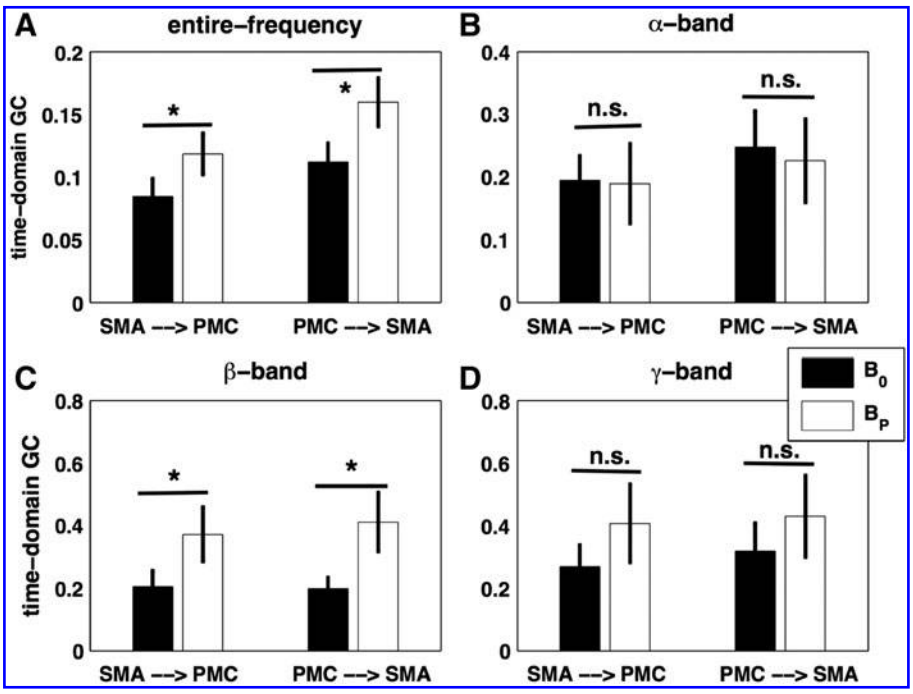

FIG. 5. Network activity between cortical EEG sources: The comparison between time-domain GC values for no button press (B_0) and button presses (B_P) obtained from **(A)** the frequency range (0.12–58 Hz), and from **(B)** α-band (8–12 Hz), **(C)** β-band (13–30 Hz), and **(D)** γ-band (30–58 Hz) separately. *$p < 0.05$; n.s., not significant. The error bar stands for the standard error of the mean.

from PMC to SMA and from SMA to PMC, significant. We calculated time-domain GC values for the entire frequency range for our calculation here (0.12–58 Hz), α-band, β-band, and γ-band (30–58 Hz) for button presses (B_P) and rest (B_0). For the entire frequency range, the causal interactions from SMA to PMC and from PMC to SMA differed significantly ($p < 0.05$). There was a greater causal influence during B_P than B_0 (Fig. 5A). These causal influences during B_P were significantly higher ($p < 0.05$) than B_0 for β-band (Fig. 5C), but not for α-band and γ-band (Fig. 5B, D). Furthermore, to investigate whether the reconstructed EEG source signals were affected by any residual volume conduction in EEG inverse source estimation, we used the procedure of time-shifting-driven signals that were used in previous studies (Adhikari et al., 2014; Faes et al., 2013; Lindner et al., 2011) to evaluate potential effects of residual volume

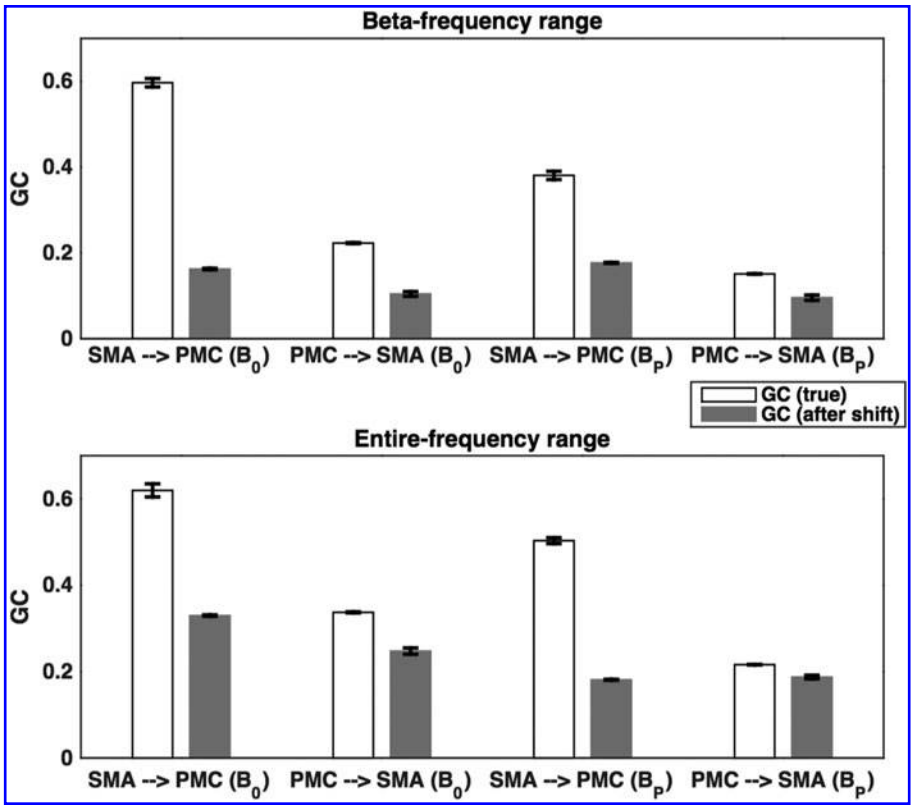

FIG. 6. Effect of any residual volume conduction in the source signals: true GC (white) and that obtained after shifting the time points (gray). All true GC values were found to be significantly greater ($p < 10^{-6}$) than the corresponding GC value obtained by shifting time points. Here time points were shifted by $t = 1, 2, 3, 4, 5$ points to generate surrogate time series and to test the hypothesis that GC would strengthen by time shifting the driven signals if volume conduction effects were present in the data.

conduction in the reconstructed source signals, to rule out the possibility that GC patterns had anything to do with volume conduction. The comparison between the maximum GC values of the original time series (for the reconstructed source waveforms) and the distribution of values obtained for a set of 50 time-shifted surrogates showed that the causal influences were not strengthened by time shifting the driven signals during B_0 and B_P (Fig. 6). The directed causal influences were not the result of volume conduction during B_0 and B_P. Figure 6 shows the causal interactions between SMA and PMC for beta-frequency (13–30 Hz) and the entire frequency range (0.12–58 Hz), and these interactions were not affected by any residual volume conduction in reconstructed source signals.

Discussion

A flow of temporal sequence of events, motor preparation, and actual execution of rhythmic tapping with precise timing mechanism are required for the generation of rhythmic movements. Previous studies on movement coordination and rhythms have shown that a complex movement involves a higher degree of central internal effort (Kelso et al., 1990; Mayville et al., 1999; Rao et al., 1993; Sakai et al., 1999). The cortical and subcortical areas involved may depend on the specific timing relationship required between motor and perceptual or imagery processes. Our fMRI results showed the areas, PMC, SMA, and Cb, involved in rhythmic motor movements and found significant unidirectional causal interactions from SMA and PMC to Cb in addition to significant bidirectional interactions between PMC and SMA during RFT tasks. Reconstructed source signals using single-trial EEG data from the cortical sources PMC and SMA showed a decrease in node activity during finger tapping compared to rest. There were significant bidirectional interactions between these nodes during RFT tasks.

Brain activations during tapping tasks

Patterns of time intervals demarcated by sensory and/or motor events called rhythms require an element of timing. We can create, maintain, and change an incredible number of slow, fast, simple, or intricate movement rhythms. The sensorimotor synchronization involved a distributed network of brain regions for the integration of sensory stimuli to motor planning and execution (Hardwick et al., 2013; Rao et al., 1997; Thaut, 2006; Thaut et al., 2008). The tap versus rest contrast showed brain activations in the left PMC, SMA, and right Cb. Different beat rhythms (B_1, B_2, B_3) versus rest (B_0) were correlated with activations in the PMC, SMA, the left basal ganglia (putamen), and the right Cb. These activation regions are consistent with previous studies (Adhikari et al., 2013; Dhamala et al., 2003; Witt et al., 2008). The SMA and motor regions are responsible for planning, higher order organization, and preparation of motor movements, whereas the primary motor area is responsible for the execution of the task (Cunnington et al., 2003; Hardwick et al., 2013; Rao et al., 1993; Roland, 1985; Samuel et al., 1998; Shibasaki and Hallett, 2006). The contralateral pre/postcentral gyrus activations are concerned with the initial cortical processing of tactile and proprioceptive information, believed to contribute to the temporal organization of motor behavior (Halsband et al., 1993; Truelle et al., 1995), and found to show pronounced activity with complexity of movement rhythms. Similar results were obtained in several other studies (Gerloff et al., 1998; Lang et al., 1990) and indicated that the premotor and supplementary motor activity is related directly to the degree to which a movement pattern must be planned. Rhythm not only activates motor areas but also helps in creating rapid motor synchronization to an external rhythmic cue in persons with and without neurological disability (Thaut et al., 1999a).

The basal ganglia, Cb, and various parts of the cortex have been shown to be involved in perceiving and generating simple to complex movement rhythms. The basal ganglia have been proposed to act as an internal clock of the brain that generates internal timing representations (Chauvigne et al., 2014) and related to sequencing aspects of rhythmic motor movements (Jueptner and Weiller, 1998; Thaut et al., 2008), whereas the Cb performs more complex timing processing, such as encoding polyrhythmic stimuli (Thaut et al., 2008), establishing the duration of discrete stimuli (Ivry and Spencer, 2004; Teki et al., 2011), or performing a correction of timing errors led by basic processing in basal ganglia (Kung et al., 2013; Teki et al., 2011). Aged subjects required more brain network activity to perform movement automatically at the same level as young subjects; age subjects not only showed greater activity in the bilateral anterior Cb, premotor area, parietal cortex, left prefrontal cortex, anterior cingulate, caudate nucleus, and thalamus but also recruited more areas, including the pre-SMA and bilateral posterior Cb compared to young subjects (Wu et al., 2005).

The cortical sensorimotor areas have been related to temporal complexity or the fine tuning of rhythms (Dhamala et al., 2003) and the sensorimotor integration for optimizing movements (Ivry, 1996; Jueptner and Weiller, 1998; Thaut et al., 2008). Putamen activations found for B_2 and B_3 (Fig. 1C, D) corresponding to the regular signal increased with increasing movement complexity (Lehericy et al., 2006). Previous studies on functional connectivity indicated that the putamen preferentially receives inputs from motor, sensory, and premotor cortices (Brooks, 1995; Graybiel et al., 1994) and is the projection site of the cortical inputs into the basal ganglia and its activity is mainly movement related instead of cognition related (Kraft et al., 2007). The cortico-basal ganglia and cortico-cerebellar circuits are involved not only in rhythmic movement generation but also in various aspects of rhythmic perception and learning (Ramnani and Passingham, 2001). Damage to these circuits impairs timing abilities (Artieda et al., 1992; Halsband et al., 1993; Mangels et al., 1998; Molinari et al., 2003), further supporting their role in rhythm perception and production (Chauvigne et al., 2014). These impairments are associated with a wide variety of neurological disorders (Allman and Meck, 2012; Hardy and Lagasse, 2013; Turgeon et al., 2012) and in abnormal sensorimotor integration in various movement disorders (Patel et al., 2014).

We found the increase in BOLD signals and decrease in alpha and beta power when subjects performed RFT tasks in comparison to rest condition. Task-induced increases of BOLD signal were observed at PMC, SMA, and Cb (Fig. 2) and decreases of EEG amplitude in alpha and beta bands (Fig. 4) were found at both PMC and SMA. These results are in good agreement with previous findings that showed an inverse functional coupling between task-induced changes of BOLD and low-frequency EEG signals (Yuan

et al., 2010). The decrease in alpha/beta activity with the complexity of the movement rhythms may be due to a decrease in the synchrony of the underlying neural population. The degree of desynchronization may be quantitatively related with an increase in neuronal activity, as reflected in the increased BOLD signal. The higher the alpha and beta desynchronization (Fig. 4), the higher is the local cortical activation (Fig. 2) found during higher beat rhythms.

Network activity

The brain activation observed in our study: PMC, SMA, Cb, premotor cortex, and putamen were consistently found in both motor imagery and motor execution tasks (Bajaj et al., 2015; Grefkes et al., 2008; Kasess et al., 2008). The core motor areas: PMC, SMA, premotor cortex are known to be connected anatomically (Pool et al., 2103; Walsh et al., 2008) and involved in planning, initiation, and execution of motor commands. Significant bidirectional causal interactions that we found between PMC and SMA during RFT tasks [from BOLD signal (Fig. 3) and from constructed EEG source signals using single-trial EEG (Fig. 5)] in our study have also been reported in several studies within these areas as well as with other areas such as basal ganglia, putamen, cerebellum, inferior and superior parietal lobule, and other somatosensory areas (Gao et al., 2011; Grefkes et al., 2008; Rehme et al., 2011; Walsh et al., 2008). We found that the RFT task is characterized by network interactions among PMC, SMA, and Cb. The Cb received significant unidirectional causal influences from cortical regions during RFT task and causal influences were found modulated with the complexity of rhythms, which may reflect the role of Cb in rhythm-information processing (D'Angelo and De Zeeuw, 2009; Salmi et al., 2010; Ziemus et al., 2007) or for the tasks involving temporal representations, situations that involved event timing (Ivry et al., 2002).

Subcortical brain areas such as putamen, globus pallidus, substantia nigra, and subthalamic nuclei and cortical motor areas such as the premotor cortex, PMC, the postparietal cortex, S1, and SMA participate in the control of motor function (Saunders et al., 2015). Impairment of motor function may lead to clinically heterogeneous signs and symptoms, observable in several clinically distinct neurological diseases and mental disorders such as schizophrenia (Hirjak et al., 2015). Abnormal neural activity in pre- and postcentral, inferior frontal, parietal, thalamic, striatal, and cerebellar structures is the indication of neurological soft signs in schizophrenia (Hirjak et al., 2015). Also, there are reports of abnormal functional activation in the cerebellum, thalamus, and cortex in patients with schizophrenia (Andreasen et al., 1996).

Our results, bidirectional interactions between SMA and PMC for the fMRI BOLD signal and reconstructed single-trial source, are consistent with the results presented in a simultaneous fNIRS, fMRI, and EEG study (Anwar et al., 2016). They have estimated the effective connectivity within cortico-cortical sensorimotor network ROIs; sensorimotor cortex (SMC), PMC, and dorsolateral prefrontal cortex (DLPFC) during finger movement tasks using fMRI (BOLD), fNIRS (oxygenated and deoxygenated hemoglobin), and EEG (scalp and source) signals. All motor tasks showed a significant bidirectional information flow among the SMC, PMC, and DLPFC, only the source level EEG GC values were significantly greater forward than the backward information flow among these ROIs. A study using MEG together with the analysis tool Dynamic Imaging of Coherent Sources (Gross et al., 2001) investigated the oscillatory network associated with simple auditory paced fingertaps (Pollok et al., 2005) and showed that the task execution was associated with a cerebello-thalamo-cortical network comprising cerebellum, thalamus, PMC, SMA, and superior temporal sulcus corresponding to the auditory cortex (Pollok et al., 2006). Significant increase in bidirectional beta-band interactions between PMC and SMA during button presses may provide information about the sensorimotor integration, including movement initiation, execution (Kuo et al., 2014), and serve as a functional link between different motor regions: PMC (Reimer and Hatsopoulos, 2010), SMA (Hosaka et al., 2016), and somatosensory cortex (Lebedev and Nelson, 1995). No significant changes in the alpha and the gamma network oscillations were found in going from simple to complex rhythms, although attenuation of the alpha power can be observed during preparation and/or execution of voluntary movements and an elevation of the gamma power over motor regions during movements of finger or other body parts (Xiao and Ding, 2015).

In summary, this simultaneous fMRI-EEG study shows that the complexity of motor rhythms is associated with network activity increases and changes in beta (13–30 Hz) band network oscillations. The analysis of the fMRI BOLD signals found brain activations in PMC, SMA, and Cb during finger movements and the network interactions were bidirectional between PMC and SMA and unidirectional to Cb from PMC and SMA. The causal interactions from PMC and SMA to Cb were modulated by the complexity of rhythm. The reconstructed single-trial EEG source signals from PMC and SMA showed the decrease in beta-power during 2-beat and 3-beat rhythms in comparison with 0-beat rhythm, but an increase in bidirectional network interactions (beta-band) between them during finger-tapping tasks in comparison to the rest. There were no significant changes in the alpha (8–12 Hz) and gamma (30–58 Hz) network oscillations in going from simple to complex rhythms. The current knowledge on motor system circuits and network interactions among motor areas during RFT task could be beneficial for mapping certain clinical symptom expressions onto distinct motor pathways.

Acknowledgments

This work was supported by the Brains and Behavior seed grant to M.D. The author M.D. acknowledges the National Science Foundation grant support (CAREER AWARD BCS 0955037).

Disclosure Statement

No competing financial interests exist.

References

Abiru M, Kikuchi Y, Tokita K, Mihara Y, Fujimoto M, Mihara B. 2008. The effects of neurologic music therapy on gait disturbance in a cerebellar ataxia: a case study. Gunma Med J 87:213–218.

Adhikari BM, Goshorn ES, Lamichhane B, Dhamala M. 2013. Temporal-order judgment of audiovisual events involves

network activity between parietal and prefrontal cortices. Brain Connect 3:536–545.
Adhikari BM, Sathian K, Epstein CM, Lamichhane B, Dhamala M. 2014. Oscillatory activity in neocortical networks during tactile discrimination near the limit of spatial acuity. Neuroimage 91:300–310.
Aguirre GK, Zarahn E, D'Esposito M. 1998. The variability of human, BOLD hemodynamic responses. Neuroimage 8:360–369.
Allen PJ, Josephs O, Turner R. 2000. A method for removing imaging artifact from continuous EEG recorded during functional MRI. Neuroimage 12:230–239.
Allen PJ, Polizzi G, Krakow K, Fish DR, Lemieux L. 1998. Identification of EEG events in the MRI scanner: the problem of pulse artifact and a method for its subtraction. Neuroimage 8: 229–239.
Allman MJ, Meck WH. 2012. Pathophysiological distortions in time perception and timed performance. Brain 135:656–677.
Andreasen NC, O'Leary DS, Cizadlo T, Arndt S, Rezai K, Ponto LL. 1996. Schizophrenia and cognitive dysmetria: a positron-emission tomography study of dysfunctional prefrontal-thalamic-cerebellar circuitry. Proc Natl Acad Sci U S A 93: 9985–9990.
Anwar AR, Muthalib M, Perrey S, Galka A, Granert O, Wolff S, et al. 2016. Effective connectivity of cortical sensorimotor networks during finger movement tasks: a simultaneous fNIRS, fMRI, EEG study. Brain Topogr 29:645–660.
Arias P, Cudeiro J. 2008. Effects of rhythmic sensory stimulation (auditory, visual) on gait in Parkinson's disease patients. Exp Brain Res 186:589–601.
Artieda J, Pastor MA, Lacruz F, Obeso JA. 1992. Temporal discrimination is abnormal in Parkinson's disease. Brain 115: 199–210.
Baccala LA, Sameshima K. 2001. Partial directed coherence: a new concept in neural structure determination. Biol Cybern 84:463–474.
Bajaj S, Butler AJ, Drake D, Dhamala M. 2015. Brain effective connectivity during motor-imagery and execution following stroke and rehabilitation. Neuroimage Clin 8:572–582.
Bernasconi C, König P. 1999. On the directionality of cortical interactions studied by structural analysis of electrophysiological recordings. Biol Cybern 81:199–210.
Bernasconi C, von Stein A, Chiang C, König P. 2000. Bi-directional interactions between visual areas in the awake behaving cat. Neuroreport 11:689–692.
Biessmann F, Plis S, Meinecke FC, Eichele T, Müller K-R. 2011. Analysis of multimodal neuroimaging data. IEEE Rev Biomed Eng 4:26–58.
Blair RC, Karniski W. 1993. An alternative method for significance testing of waveform difference potentials. Psychophysiology 30:518–524.
Brooks DJ. 1995. The role of the basal ganglia in motor control: contributions from PET. J Neurol Sci 128:1–13.
Brovelli A, Ding M, Ledberg A, Chen Y, Nakamura R, Bressler SL. 2004. Beta oscillations in a large-scale sensorimotor cortical network: directional influences revealed by Granger causality. Proc Natl Acad Sci USA 101:9849–9854.
Brown S, Martinex MJ, Parsons LM. 2006. The neural basis of human dance. Cereb Cortex 16:1157–1167.
Buchel C, Friston KJ. 1997. Modulation of connectivity in visual pathways by attention: cortical interactions evaluated with structural equation modelling and fMRI. Cereb Cortex 7:768–778.
Chauvigne LA, Gitau KM, Brown S. 2014. The neural basis of audiomotor entrainment: an ALE meta-analysis. Front Hum Neurosci 8:776.
Cox RB. 1996. AFNI: software for analysis and visualization of functional magnetic resonance neuroimages. Comput Biomed Res 29:162–173.
Cox RW, Reynolds RC, Taylor PA. 2016. FMRI clustering in AFNI: false-positive rates redux. Brain Connect 7:152–171.
Cunnington R, Windischberger C, Deecke L, Moser E. 2003. The preparation and readiness for voluntary movement: a high-field event-related fMRI study of the Bereitschafts-BOLD response. Neuroimage 20:404–412.
D'Angelo E, De Zeeuw CI. 2009. Timing and plasticity in the cerebellum: focus on the granular layer. Trends Neurosci 32:30–40.
David O, Guillemain I, Saillet S, Reyt S, Deransart C, Segebarth C, Depaulis A. 2008. Identifying neural drivers with functional MRI: an electrophysiological validation. PLoS Biol 6:2683–2697.
de l'Etoile SK. 2008. The effect of rhythmic auditory stimulation on the gait parameters of patients with incomplete spinal cord injury: an exploratory pilot study. Int J Rehabil Res 31:155–157.
de Souza ACS, Yehia HC, Sato M-A, Callan D. 2013. Brain activity underlying auditory perceptual learning during short period training: simultaneous fMRI and EEG recording. BMC Neurosci 14:8.
Debener S, Strobel A, Sorger B, Peters J, Kranczioch C, Engel AK, Goebel R. 2007. Improved quality of auditory event-related potentials recorded simultaneously with 3-T fMRI: removal of the ballistocardiogram artefact. Neuroimge 34: 587–597.
Debener S, Ullsperger M, Siegel M, Engel K. 2006. Single-trial EEG-fMRI reveals the dynamics of cognitive function. Trends Cogn Sci 10:558–563.
Dhamala M, Pagnoni G, Wiesenfeld K, Zink CF, Martin M, Berns GS. 2003. Neural correlates of the complexity of rhythmic finger tapping. Neuroimage 20:918–926.
Dhamala M, Rangarajan G, Ding M. 2008. Analyzing information flow in brain networks with nonparametric Granger causality. Neuroimage 41:354–362.
Faes L, Nollo G, Porta A. 2013. Compensated transfer entropy as a tool for reliably estimating information transfer in physiological time series. Entropy 15:198–219.
Fazli S, Mehnert J, Steinbrink J, Curio G, Villringer A, Müller K, Blankertz B. 2012. Enhanced performance by a hybrid NIRS-EEG brain computer interface. Neuroimage 59:519–529.
Friston KJ. 2009. Modalities, modes, and models in functional neuroimaging. Science 326:399–403.
Friston KJ, Buchel C. 2000. Attentional modulation of effective connectivity from V2 to V5/MT in humans. Proc Natl Acad Sci U S A 97:7591–7596.
Friston KJ, Frith CD, Liddle PF, Frackowiak RSJ. 1993. Functional connectivity: the principle component analysis of large (PET) data sets. J Cereb Blood Flow Metab 13:5–14.
Friston KJ, Harrison L, Penny W. 2003. Dynamic causal modeling. Neuroimage 19:1273–1302.
Friston KJ, Holmes L, Worsely KJ, Poline JB, Firth CD, Frackowiak RSJ. 1995. Statistical parametric maps in functional imaging: a general linear approach. Hum Brain Mapp 2: 189–210.
Gao Q, Duan X, Chen H. 2011. Evaluation of effective connectivity of motor areas during motor imagery and execution using conditional Granger causality. Neuroimage 54:1280–1288.

Gerloff C, Richard J, Hadley J, Schulman AE, Honda M, Hallett M. 1998. Functional coupling and regional activation of human cortical motor areas during simple, internally paced and externally paced finger movements. Brain 121:1513–1531.

Goebel R, Roebroeck A, Kim D, Formisano E. 2004. *Directed Cortical Interactions During Dynamic Sensory-Motor Mapping.* New York: Oxford University Press.

Goebel R, Roebroeck A, Kim DS, Formisano E. 2003. Investigating directed cortical interactions in time-resolved fMRI data using vector autoregressive modeling and Granger causality mapping. Magn Reson Imaging 21:1251–1261.

Granger CWJ. 1969. Investigating causal relations by econometric models and cross-spectral methods. Econometrica 37: 424–438.

Granger CWJ. 1980. Testing for causality: a personal viewpoint. J Econ Dyn Control 2:329–352.

Graybiel AM, Aosaki T, Flaherty AW, Kimura M. 1994. The basal ganglia and adaptive motor control. Science 265: 1826–1831.

Grefkes C, Eickhoff SB, Nowak DA, Dafotakis M, Fink GR. 2008. Dynamic intra- and interhemispheric interactions during unilateral and bilateral hand movements assessed with fMRI and DCM. Neuroimage 41:1382–1394.

Gross J, Kujala J, Hamalainen M, Timmermann L, Schnitzler A, Salmelin R. 2001. Dynamic imaging of coherent sources: studying neural interactions in the human brain. Proc Natl Acad Sci U S A 98:694–699.

Haken H. 1996. *Principles of Brain Functioning: A Synergetic Approach to Brain Activity, Behavior, and Cognition.* Berlin: Springer.

Halsband U, Ito N, Tanji J, Freund HJ. 1993. The role of premotor cortex and the supplementary motor area in the temporal control of movement in man. Brain 116:243–266.

Hamalainen M, Ilmoniemi RJ. 1994. Interpreting magnetic fields of the brain: minimum norm estimates. Med Biol Eng Comput 32:35–42.

Handwerker DA, Ollinger JM, D'Esposito M. 2004. Variation of BOLD hemodynamic responses across subjects and brain regions and their effects on statistical analyses. Neuroimage 21: 1639–1651.

Hardwick RM, Rottschy C, Miall RC, Eickhoff SB. 2013. A quantitative meta-analysis and review of motor learning in the human brain. Neuroimage 67:283–297.

Hardy MW, Lagasse AB. 2013. Rhythm, movement, and autism: using rhythmic rehabilitation research as a model for autism. Front Integr Neurosci 7:19.

Harrison L, Penny WD, Friston KJ. 2003. Multivariate autoregressive modeling of fMRI time series. Neuroimage 19: 1477–1491.

Hayden R, Clair AA, Johnson G, Otto D. 2009. The effect of rhythmic auditory stimulation (RAS) on physical therapy outcomes for patients in gait training following stroke: a feasibility study. Int J Neurosci 119:2183–2195.

Hesse W, Moller E, Arnold M, Schack B. 2003. The use of time-variant EEG Granger causality for inspecting directed interdependencies of neural assemblies. J Neurosci Methods 124:27–44.

Hirjak D, Thomann PA, Kubera KM, Wolf ND, Sambataro F, Wolf RC. 2015. Motor dysfunction within the schizophrenia-spectrum: a dimensional step towards an underappreciated domain. Schizophr Res 169:217–233.

Hosaka R, Nakajima T, Aihara K, Yamaguchi Y, Mushiake H. 2016. The suppression of beta oscillations in the primate supplementary motor complex reflects a volatile state during the updating of action sequences. Cereb Cortex 26:3442–3452.

Howe TE, Lovgreen B, Cody FW, Ashton VJ, Oldham JA. 2003. Auditory cues can modify the gait of persons with early-stage Parkinson's disease: a method for enhancing Parkinsonian walking performance? Clin Rehabil 17:363–367.

Hu M, Liang H. 2014. A copula approach to assessing Granger causality. Neuroimage 100:125–134.

Hurt CP, Rice RR, McIntosh GC, Thaut MH. 1998. Rhythmic auditory stimulation in gait training for patients with traumatic brain injury. J Music Ther 35:228–241.

Iannetti GD, Niazy RK, Wise RG, Jezzard P, Brooks JC, Zambreanu L, et al. 2005. Simultaneous recording of laser-evoked brain potentials and continuous, high-field functional magnetic resonance imaging in humans. Neuroimage 28:708–719.

Ivry RB. 1996. The representation of temporal information in perception and motor control. Curr Opin Neurobiol 6:851–857.

Ivry RB, Spencer RM, Zelaznik HN, Diedrichsen J. 2002. The cerebellum and event timing. Ann N Y Acad Sci 978:302–317.

Ivry RB, Spencer RMC. 2004. The neural representation of time. Curr Opin Neurobiol 14:225–232.

Jueptner M, Weiller C. 1998. A review of differences between basal ganglia and cerebellar control of movements as revealed by functional imaging studies. Brain 121:1437–1449.

Kaminski M, Ding M, Truccolo WA, Bressler SL. 2001. Evaluating causal relations in neural systems: granger causality, Directed Transfer Function (DTF) and statistical assessment of significance. Biol Cybern 85:145–157.

Kasess CH, Windischberger C, Cunnington R, Lanzenberger R, Pezawas L, Moser E. 2008. The suppressive influence of SMA on M1 in motor imagery revealed by fMRI and dynamic causal modeling. Neuroimage 40:828–837.

Kelso JAS. 1995. *Dynamic Patterns: the Self-Organization of Brain and Behavior.* Cambridge, MA: MIT Press.

Kelso JAS, DelColle JD, Schoner G. 1990. *Action-Perception as a Pattern Formation Process.* Hillsdale, NJ: Erlbaum.

Kenyon GP, Thaut MH. 2000. A measure of kinematic limb instability modulation by rhythmic auditory stimulation. J Biomech 33:1319–1323.

Kraft E, Chen AW, Flaherty AW, Blood AJ, Kwong KK, Jenkins BG. 2007. The role of the basal ganglia in bimanual coordination. Brain Res 1151:62–73.

Kung S-J, Chen JL, Zatorre RJ, Penhune VB. 2013. Interacting cortical and basal ganglia networks underlying finding and tapping to the musical beat. J Cogn Neurosci 25:401–420.

Kuo CC, Luu P, Morgan KK, Dow M, Davey C, Song J, et al. 2014. Localizing movement-related primary sensorimotor cortices with multi-band EEG frequency changes and functional MRI. PLoS One 9:e112103.

Lang W, Obrig H, Lindinger G, Cheyne D, Deecke L. 1990. Supplementary motor area activation while tapping bimanually different rhythms in musicians. Exp Brain Res 79:504–514.

Lebedev MA, Nelson RJ. 1995. Rhythmically firing (20–50 Hz) neurons in monkey primary somatosensory cortex: activity patterns during initiation of vibratory-cued hand movements. J Comput Neurosci 2:313–334.

Lehericy S, Bardinet E, Tremblay L, Van de Moortele PF, Pochon JB, Dormont D, et al. 2006. Motor control in basal

ganglia circuits using fMRI and brain atlas approaches. Cereb Cortex 16:149–161.

Lewis PA, Wing AM, Pope PA, Praamstra P, Miall RC. 2004. Brain activity correlates differentially with increasing temporal complexity of rhythms during initialization, synchronization, and continuation phases of paced finger tapping. Neuropsychologia 42:1301–1312.

Liang H, Ding M, Nakamura R, Bressler SL. 2000. Causal influences in primate cerebral cortex during visual pattern discrimination. NeuroReport 11:2875–2880.

Liang H, Gong X, Chen M, Yan Y, Li W, Gilbert CD. 2017. Interactions between feedback and lateral connections in the primary visual cortex. Proc Natl Acad Sci U S A pii: 201706183.

Lindner M, Vicente R, Priesemann V, Wibral M. 2011. TRENTOOL: a Matlab open source toolbox to analyse information flow in time series data with transfer entropy. BMC Neurosci 12:119.

Liu Z, Ding L, He B. 2006. Integration of EEG/MEG with MRI and fMRI in functional neuroimaging. IEEE Eng Med Biol Mag 25:46–53.

Mangels JA, Irvy RB, Shimizu N. 1998. Dissociable contributions of the prefrontal and neocerebellar cortex to time perception. Cogn Brain Res 7:15–39.

Mayville JM, Bressler SL, Fuchs A, Kelso JAS. 1999. Spatiotemporal reorganization of electrical activity in the human brain associated with a timing transition in rhythmic auditory-motor coordination. Exp Brain Res 127:371–381.

McIntosh AR, Gonzalez-Lima F. 1994. Structural equation modeling and its application to network analysis in functional brain imaging. Hum Brain Mapp 2:2–22.

McIntosh GC, Brown SH, Rice RR, Thaut MH. 1997. Rhythmic auditory-motor facilitation of gait patterns in patients with Parkinson's disease. J Neurol Neurosurg Psychiatry 62: 22–26.

Meyer P, Hoppstaedter M, Baeuchl C, Zangl M, Diener C, Flor H. 2011. The N400 reflects activity in the anterior medial temporal lobe (AMTL): simultaneous EEG-fMRI reveals the neural correlates of semantic priming. Psychophysiology 48:S52.

Molinari M, Leggio MG, De Martin M, Ceresa A, Thaut M. 2003. Neurobiology of rhythmic motor entrainment. Ann NY Acad Sci 999:313–321.

Niazy RK, Beckmanna CF, Iannetti GD, Brady JM, Smith SM. 2005. Removal of FMRI environment artifacts from EEG data using optimal basis sets. Neuroimage 28:720–737.

Novitskiy N, Ramautar JR, Vanderperren K, De Vos M, Mennes M, Mijovic B, et al. 2011. The BOLD correlates of the visual P1 and N1 in single-trial analysis of simultaneous EEG-fMRI recordings during a spatial detection task. Neuroimage 54: 824–835.

Ostwald D, Porcaro C, Bagshaw AP. 2011. Voxel-wise information theoretic EEG-fMRI feature integration. Neuroimage 55: 1270–1286.

Patel N, Jankovic J, Hallett M. 2014. Sensory aspects of movement disorders. Lancet Neurol 13:100–112.

Pollok B, Gross J, Muller K, Aschersleben G, Schnitzler A. 2005. The cerebral oscillatory network associated with auditorily paced finger movements. Neuroimage 24:646–655.

Pollok B, Gross J, Schnitzler A. 2006. How the brain controls repetitive finger movements. J Physiol Paris 99:8–13.

Pool EM, Rehme AK, Fink GR, Eickhoff SB, Grefkes C. 2103. Network dynamics engaged in the modulation of motor behavior in healthy subjects. Neuroimage 82:68–76.

Prassas SG, Thaut MH, McIntosh GC, Rice RR. 1997. Effect of auditory rhythmic cuing on gait kinematic parameters in stroke patients. Gait Posture 6:218–223.

Ramnani N, Passingham RE. 2001. Changes in the human brain during rhythm learning. J Cogn Neurosci 13:952–966.

Rao SM, Binder JR, Bandettini PA, Hammeke TA, Yetkin FZ, Jesmanowicz A, et al. 1993. Functional magnetic resonance imaging of complex human movements. Neurology 43: 2311–2318.

Rao SM, Harrington DL, Haaland KY, Bobholz JA, Cox RA, Binder JR. 1997. Distributed neural systems underlying the timing of movements. J Neurosci 17:5528–5535.

Rehme AK, Eickhoff SB, Wang LE, Fink GR, Grefkes C. 2011. Dynamic causal modeling of cortical activity from the acute to the chronic stage after stroke. Neuroimage 55:1147–1158.

Reimer J, Hatsopoulos NG. 2010. Periodicity and evoked responses in motor cortex. J Neurosci 30:11506–11515.

Rochester L, Burn DJ, Woods G, Godwin J, Nieuwboer A. 2009. Does auditory rhythmical cueing improve gait in people with Parkinson's disease and cognitive impairment? A feasibility study. Mov Disord 24:839–845.

Roebroeck A, Formisano E, Goebel R. 2011. The identification of interacting networks in the brain using fMRI: model selection, causality and deconvolution. Neuroimage 58:296–302.

Roelstraete B, Rosseel Y. 2012. Does partial Granger causality really eliminate the influence of exogenous inputs and latent variables? J Neurosci Methods 206:73–77.

Roerdink M, Lamoth CJC, Kwakkel G, van Wieringen PCW, Beek PJ. 2007. Gait coordination after stroke: benefits of acoustically paced treadmill walking. Phys Ther 87:1009–1022.

Roerdink M, Lamoth CJC, van Kordelaar J, Elich P, Konijnenbelt M, Kwakkel G, Beek PJ. 2009. Rhythm perturbations in acoustically paced treadmill walking after stroke. Neurorehabil Neural Repair 23:668–678.

Roland PE. 1985. Cortical organization of voluntary behavior in man. Neurobiology 4:155–167.

Sakai K, Hikosaka O, Miyauchi S, Takino R, Tamada T, Iwata NK, Nielsen M. 1999. Neural representation of a rhythm depends on its interval ratio. J Neurosci 19:10074–10081.

Salmi J, Pallesen KJ, Neuvonen T, Brattico E, Korvenoja A, Salonen O, Carlson S. 2010. Cognitive and motor loops of the human cerebro-cerebellar system. J Cogn Neurosci 22: 2663–2676.

Sammer G, Blecker C, Gebhardt H, Kirsch P, Stark R, Vaitl D. 2005. Acquisition of typical EEG waveforms during fMRI: SSVEP, LRP, and frontal theta. Neuroimage 24:1012–1024.

Samuel M, Williams S, Leigh P, Simmons A, Chakraborti S, Andrew C, et al. 1998. Exploring the temporal nature of hemodynamic responses of cortical motor areas using functional MRI. Neurology 51:1567–1575.

Sato JR, Junior EA, Takahashi DY, de Maria Felix M, Brammer MJ, Morettin PA. 2006. A method to produce evolving functional connectivity maps during the course of an fMRI experiment using wavelet-based time-varying Granger causality. Neuroimage 31:187–196.

Saunders A, Oldenburg IA, Berezovskii VK, Johnson CA, Kingery ND, Elliott HL, et al. 2015. A direct GABAergic output from the basal ganglia to frontal cortex. Nature 521:85–89.

Schaal S, Sternad D, Osu R, Kawato M. 2004. Rhythmic arm movement is not discrete. Nat Neurosci 7:1136–1143.

Shibasaki H. 2008. Human brain mapping: hemodynamic response and electrophysiology. Clin Neurophysiol 119:731–743.

Shibasaki H, Hallett M. 2006. What is the Bereitschaftspotential? Clin Neurophysiol 117:2341–2356.

Teki S, Grube M, Griffiths TD. 2011. A unified model of time perception accounts for duration-based and beat-based timing mechanisms. Front Integr Neurosci 5:90.

Thaut MH. 2006. Neural basis of rhythmic timing networks in the human brain. Ann N Y Acad Sci 999:364–373.

Thaut MH, Demartin M, Sanes JN. 2008. Brain networks for integrative rhythm formation. PLoS One 3:e2312.

Thaut MH, Kenyon GP, Schauer ML, McIntosh GC. 1999a. The connection between rhythmicity and brain function: implications for therapy of movement disorders. Eng Med Biol Mag 18:101–108.

Thaut MH, McIntosh GC, Rice RR, Miller RA, Rathbun J, Brault JM. 1996. Rhythmic auditory stimulation in gait training for Parkinson's disease patients. Mov Disord 11:193–200.

Thaut MH, Miltner R, Lange HW, Hurt CP, Hoemberg V. 1999b. Velocity modulation and rhythmic synchronization of gait in Huntington's disease. Mov Disord 14:808–819.

Truelle JL, Le GD, Joseph PA, Aubin G, Derouesne C, Lezak MD. 1995. Movement disturbances following frontal lobe lesions: qualitative analysis of gesture motor programming. Neuropsychiatry Neuropsychol Behav Neurol 8:14–19.

Turgeon M, Giersch A, Delevoye-Turrell Y, Wing AM. 2012. Impaired predictive timing with spared time interval production in individual with schizophrenia. Psychiatry Res 197: 13–18.

Ullsperger M. 2010. EEG-informed fMRI analysis. In: Ullsperger M, Debener S (eds.) *Simultaneous EEG and fMRI: Recording, Analysis, and Application.* New York: Oxford University Press; pp. 153–159.

Ullsperger M, von Cramon DY. 2001. Subprocesses of performance monitoring: a dissociation of error processing and response competition revealed by event-related fMRI and ERPs. Neuroimage 14:1387–1401.

Valdes-Sosa PA, Roebroeck A, Daunizeau J, Friston K. 2011. Effective connectivity: influence, causality and biophysical modeling. Neuroimage 58:339–361.

Verstynen T, Diedrichsen J, Albert N, Aparicio P, Ivry RB. 2005. Ipsilateral motor cortex activity during unimanual hand movements relates to task complexity. J Neurophysiol 93:1209–1222.

Walsh RR, Small SL, Chen EE, Solodkin A. 2008. Network activation during bimanual movements in humans. Neuroimage 43:540–553.

Wang J-Z, Williamson SJ, Kufman L. 1992. Magnetic source images determined by 934 a lead-field analysis: the unique minimum-norm least-squares estimation. IEEE Trans Biomed Eng 56:111–121.

Witt ST, Laird AR, Meyerand ME. 2008. Functional neuroimaging correlates of finger-tapping task variations: an ALE meta-analysis. Neuroimage 42:343–356.

Wu GR, Liao W, Stramaglia S, Ding JR, Chen H, Marinazzo D. 2013. A blind deconvolution approach to recover effective connectivity brain networks from resting state fMRI data. Med Image Anal 17:365–374.

Wu T, Hallet M. 2005. The influence of normal human ageing on automatic movements. J Physiol 562:605–615.

Xiao R, Ding L. 2015. EEG resolutions in detecting and decoding finger movements from spectral analysis. Front Neurosci 9:308.

Yuan H, Liu T, Szarkowski R, Rios C, Ashe J, He B. 2010. Negative covariation between task-related responses in alpha/beta-band activity and BOLD in human sensorimotor cortex: an EEG and fMRI study of motor imagery and movements. Neuroimage 49:2596–2606.

Ziemus B, Baumann O, Luerding R, Schlosser R, Schuierer G, Bogdahn U, Greenlee MW. 2007. Impaired working-memory after cerebellar infarcts paralleled by changes in BOLD signal of a cortico-cerebellar circuit. Neuropsychologia 45: 2016–2024.

Address correspondence to:
Bhim M. Adhikari
Department of Psychiatry
Maryland Psychiatric Research Center
University of Maryland School of Medicine
Baltimore, MD 21228

E-mail: bhimdhkr@gmail.com